Network-Independent Grid Synchronous Stability Boundary and Spontaneous Synchronization

Yu Yuan *

Posted Date: 16 January 2025

doi: 10.20944/preprints202310.1791.v6

Keywords: Stability boundary; Synchronization; complex network

Article

Network-Independent Synchronous Stability Boundary and Spontaneous Synchronization

Yu Yuan

SICHUAN TECHNOLOGY & BUSINESS COLLEGE, China; yuyuan.sctbc@outlook.com

Abstract: Synchronization of complex networks has been widely studied. Current research on the synchronization of complex networks is based on concepts from graph theory and statistical physics. However, the study of real network synchronization remains present substantial obstacles. To overcome the difficulties caused by the complexity of the network, I report a simple synchronization stability boundary equation and identify a spontaneous synchronization structure in power grids for the first time. The findings indicate that both the synchronization stability boundary and the location of spontaneous synchronization occurred are independent of the network. The boundary equation harmonizes two contradictory conclusions well and reveals the mechanism of the synchronization of different individuals through coupling. These results offer a new direction for synchronization research, providing a means to overcome the challenges posed by network complexity, nonlinearity, and uncertainty, and enabling a unified approach to analyzing the synchronization stability of grids.

Keywords: stability boundary; Synchronization; complex network

Introduction

The study of synchronization began with Huygens. As the number of studies on collective behavior in complex systems has grown, synchronization in coupled systems has garnered extensive attention[1]. Synchronization in complex systems[2], e.g., synchronous discharge, the flashing of fireflies, and the synchronization of generators, is widely observed in nature and industry.

It is widely believed that networks are closely related to spontaneous synchronization[2]. Current research on the synchronization of complex networks is based on concepts from graph theory and statistical physics, such as the connectivity of the graph and the nodal degree[2]. To analyze synchronization behaviors of complex networks, these approaches require clear information about the network structure and simplify the interactions between individuals into a coupled network. However, this is difficult to achieve in practice[3,4], as realistic interactions often cannot be observed. The complexity of real networks can also make topological information incomplete[5]. Additionally, overly large networks make clear topology modeling quite difficult. These challenges can lead to incorrect network reconfiguration and link predictions. Even if complete information regarding the network topology is obtained, other difficulties, such as the diversity of networks and community structures, uncertain dynamics and nonlinear network parameters, are often encountered simultaneously in real networks. These difficulties present substantial obstacles for the study of network synchronization.

To overcome the abovementioned difficulties, a network-independent synchronization analysis path is constructed for generator synchronization in power systems in this paper. Power systems are the largest man-made systems and are considered to be typical complex network systems. Therefore, the study of the synchronization behavior of generators in power grids is of critical importance not only for the stable operation of power systems but also for the wider field of synchronization of complex networks[1,2]. The approach in this paper identifies collective synchronization and those individuals not participating in it, based solely on the behavior of each individual in the system. In particular, this method reveals how individuals in the network are synchronized while ignoring the

 doi:10.20944/preprints202310.1791.v6

network structure. This approach has been experimentally verified for the realistic power grid systems.

Synchronization is a prerequisite for the normal operation of a power grid[6]. Large power systems are complex coupled systems where nonlinearities and uncertainties coexist[7]. To analyze the synchronization of generators, numerous insightful methods are being developed[1,8–12], including the determination of synchronous stability boundaries[13–15] and the use of spontaneous synchronization conditions[2].

The identification of the synchronous stability boundary of a system is a key unresolved problem[14,16,17]. A stablity boundary is the union of critical points[18], and when the system state is outside the stability boundary, it is desynchronized[15]. The boundary, which is a core concept of grid stability, is closely related to many other issues encountered in power systems[19–21]. Therefore, investigations of synchronous stability boundaries can make a significant impact on the development of power systems and the synchronization stability of complex networks. The derivation of an analytical equation that can describe a boundary has been a long-standing research goal in the field of power systems[13,14,22]. However, current research is still limited by the nonlinearity and uncertainty of power systems. On the other hand, the spontaneous synchronization of complex systems has been utilized to elucidate the synchronized operation of generators in interconnected grids[23]. Therefore, many studies on power system stability are based on the knowledge of synchronization conditions of complex networks[2,23,24]. However, this scheme is in some cases considered to oversimplify real systems[9,23], and it has been argued that self-organization is not relevant for a power grid[9].

Here, an equation is derived and visualized based on a succinct consensus. The equation describes the synchronous stability boundary of a power system in a unified manner and has elegant formal and physical interpretations. I started by showing the validity of the boundary equation with three pieces of evidences. These evidences demonstrate that this approach addresses the problems of the multiswing stability discrimination of multiple generators in a power system and partial synchronization. Subsequently, I demonstrated that the synchronous stability boundary is independent of the network structure and parameters. It is also shown here that the synchronization stability of the power system is determined by the amplitude, while the conclusion that both symmetry and asymmetry promote synchronization is discussed. In addition, by comparing the boundary with the location of synchronization occurred, I observed that spontaneous synchronization occurs only close to the boundary and is manifested as a specific structure. This represents the first clear evidence of spontaneous synchronization in a power system. Moreover, this close connection suggests that, like the synchronous stability boundary, the spontaneous synchronization on a network is also not directly related to the network. This novel approach is developed to investigate the synchronization of complex networks, taking into account potential scenarios of realistic network complexity, nonlinearity, or uncertainty. The conclusion in this paper may inspire advances in other disciplines.

Stability Boundary

Synchronization occurs when the coupling dominates the dissimilarity[2]. Currently[2], the coupling is typically quantified by graph theory, and the dissimilarity is quantified by the frequencies ω_i. In this work, it is assumed that the coupling is quantified by the coupling power and the dissimilarity is quantified by the dissimilar power. When the generators are synchronized, there is no dissimilarity, meaning the dissimilar power is 0. The coupling power is denoted as $P_{\Delta u}$ and the dissimilar power is denoted as $P_{\partial u}$. That is, when $P_{\Delta u} \geq P_{\partial u}$, the system is synchronous and stable, otherwise it is out of synchronization. Therefore, $P_{\Delta u} = P_{\partial u}$ represents the synchronous stability boundary. This assumption quantifies the interactions between individuals and is not based on graph theory or statistical physics concepts.

 doi:10.20944/preprints202310.1791.v6

The boundary equation is expressed as follows:

$$\left(|u_K| = |u_L|\right) \cup \left(\frac{|u_L|}{|u_K|} = 2\cos\delta_{K,L} - 1 \right) \quad (1)$$

where $|u_K| > |u_L| \geq 0, |\delta_{K,L}| \geq 0$. Eq. (1) is the specific expression of $P_{\Delta u} = P_{\partial u}$ in the power system.

Here, u_K, u_L denote the voltages per unit of the Kth and Lth meta-generators, respectively. The amplitude, which in this context refers to voltage, has been previously overlooked for simplicity[9,23] but is crucial for the synchronization stability of the grid. ω_i is the rotor speed per unit of the ith meta-generator, which is a normalization quantity commonly used in power system studies. $\delta_K = 2\arctan(\omega_K)$ is defined as the angle of rotation rate of the Kth meta-generator. The angle difference of rotation rate between the Kth and Lth meta-generators is $\delta_{K,L} = |\delta_K - \delta_L| \geq 0$. It is important to note that δ_K is not a phase and that $L = K + 1$. According to the definition of synchronization, $\delta_1 = \cdots = \delta_K = \delta_L = \cdots = \delta_n$.

(a). Visualization of the stability boundary. The stability boundary in Eq. (1) (blue surface and dark green plane) and the pink planes $0 - u_L - \delta_{K,L}$, $u_K - 0 - \delta_{K,L}$ and $u_K - u_L - 0$ collectively define the boundaries and enclose the stability domain.

(b). Synchronization stabilization discrimination. The dark green plane is not shown. Δt is the fault clearing time. $(u_K, u_L, \delta_{K,L})$ is defined as the coordinate of the coupling point of the Kth and Lth meta-generators, and it is computed from u_K, δ_K, u_L and δ_L. $d(\Delta t) = 0.155\ s - 0.154\ s = 0.001\ s$ denotes the step length commonly used in power system studies. The coupling points in panel (b) are calculated using Eqs. (S3) and (S4).

(c). The disturbed trajectory of $(u_1, u_2, \delta_{1,2})$ ($\Delta t = 0.155\ s$). Each cyan point represents the mean position of $(u_1, u_2, \delta_{1,2})$ for a period of 1 second. The time T=8 s and the time interval $dT = 1s$ are defined in Eq. (S5).

(d) and (e). The results of the numerical experiment. The horizontal axis represents the time. The maximum value of $\delta_i(t)$ is represented by the magenta curve, and the minimum value is represented by the cyan curve. $\delta_{\min}(t) \leq \delta_i(t) \leq \delta_{\max}(t)$. At 11 second, $\delta_{\max}(t) - \delta_{\min}(t) \approx 1°$ in (d), and $\delta_{\max}(t) - \delta_{\min}(t) \approx 14°$ in (e). As illustrated in panel (d), the $\delta_i(t)$ values of all meta-generators are close to each other and have approximately the same rate of change. panel (e) shows that in the time interval $(9\ s, 10\ s)$, $\delta_{\max}(t) - \delta_{\min}(t)$ increases sharply, indicating generator desynchronization.

(f). The phenomenon of partial synchronization and the stability of multiple swings for multiple generators. $\Delta t = 0.155\ s$. After approximately 9 seconds, meta-generator 1 disengages from the cluster (cyan line). Subsequently, meta-generators 10 (magenta line) and 2 (orange dashed line) are separated. Meta-generators 3~9 form a synchronized cluster (green lines). $\delta_i(t)$ in panels (d), (e) and (f) are calculated using simulation software and Eq. (S2).

Three pieces of evidence demonstrate that Eq. (1) effectively describes the synchronization stability boundary: 1) the boundary effectively distinguishes between stable and unstable states of the power system [see Figures. 1(b) and S1(a)], 2) the stability of multiple swings [see Figures 1(c) and S1(b)], and 3) the partial synchronization phenomenon [see Figures 1(f) and S1(e)].

Figure 1(b) illustrates that the synchronization stability boundary effectively differentiates between synchronized and desynchronized states.. A system comprising n meta-generators possesses n-1 coupling points. The behavior of the cyan and magenta dots is significantly different,

 doi:10.20944/preprints202310.1791.v6

despite the slight difference in Δt (Figure 1(b)). When $\Delta t = 0.154\ s$, all of the cyan coupling points are clustered at the boundary. When $\Delta t = 0.155\ s$, the three magenta coupling points, i.e., $(u_1, u_2, \delta_{1,2})$, $(u_2, u_3, \delta_{2,3})$, and $(u_9, u_{10}, \delta_{9,10})$, are outside the boundary and away from the rest of points. As mentioned above, when $P_{\Delta u} < P_{\partial u}$, the coupling point $(u_K, u_L, \delta_{K,L})$ is outside the boundary and the power system is out of synchronization. Consequently, it is concluded that the system is stable at $\Delta t = 0.154\ s$ and out of synchronization at $\Delta t = 0.155 s$. The results in Figures 1(d) and (e) are in good agreement with this conclusion. Additional analogous results can be found in Figure S8.

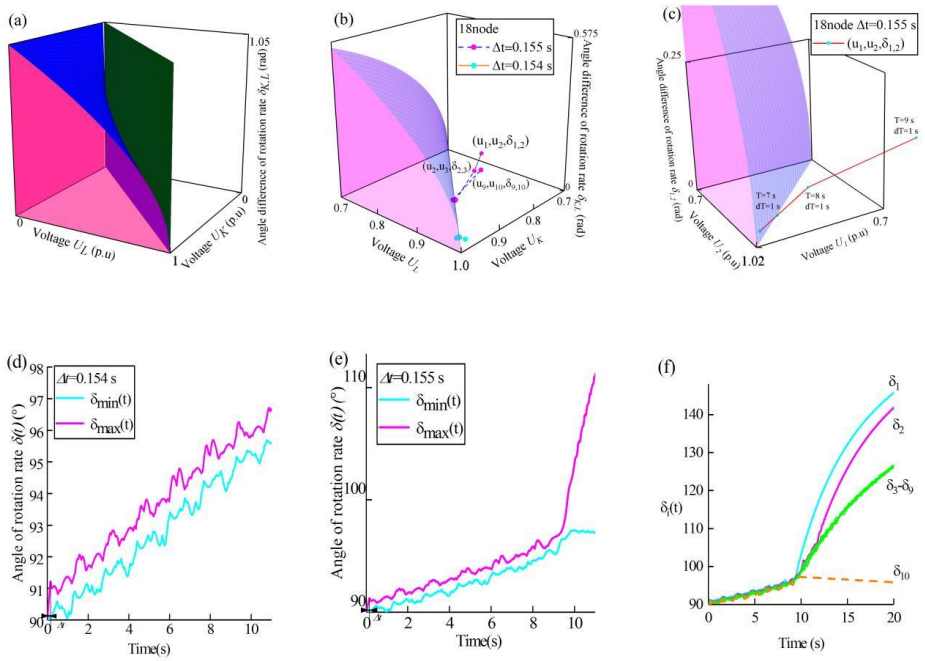

Figure 1. Stability boundary. A New England test system (10-gen) was used. A three-phase short-circuit ground fault occurred at node 18.

Furthermore, utilizing Figure 1(b) facilitates easily identify different synchronization patterns as it provides specific information about synchronized and desynchronized individual meta-generators or groups of meta-generators. The New England test system comprises 10 meta-generators, which is equivalent to 9 coupling points. As shown in Figure 1(b), the 3 coupling points $(u_1, u_2, \delta_{1,2})$, $(u_2, u_3, \delta_{2,3})$ and $(u_9, u_{10}, \delta_{9,10})$ are outside the boundary while the rest of the points are clustered near the boundary. This signify that the meta-generators are divided into 4 synchronization groups. Specifically, $(u_1, u_2, \delta_{1,2})$ outside the boundary means that the meta-generators 1 and 2 are not synchronized. There are analogous conclusions for $(u_2, u_3, \delta_{2,3})$ and $(u_9, u_{10}, \delta_{9,10})$. That is, the meta-generators numbered 1, 2 and 10 are out of synchronization while the other meta-generators remain synchronized. This indicates that the meta-generators in each group are also clearly shown in Figure 1(b). The result for the meta-generator synchronization group shown in Figure 1(f) is in good agreement with those presented in Figure 1(b). This is the phenomenon of partial synchronization. These results suggest that the partial synchronization phenomenon[25–28] is caused by the loss of synchronization stability among these individuals or groups. This interpretation will deepen our understanding of the complex phenomenon of partial synchronization.

 doi:10.20944/preprints202310.1791.v6

Figure 1(c) clearly shows the transition of the power system from stabilization to instability. As shown in Figure 1(c), $(u_1, u_2, \delta_{1,2})$ crosses the boundary outwardly during the time interval $(8s,9s)$. Subsequently, $\delta_{1,2}$ increases dramatically during the time interval $(9\,s, 10\,s)$. These results are in good agreement with the simulation result presented in Figure 1(e). The simulation result demonstrates that the system loses synchronization during the aforementioned time interval. Therefore, the time at which the coupling point crosses the boundary is the onset of synchronization loss. These results pertain to the stability of multiple swings for multiple generators, an important issue that has not been resolved to date[29,30]. The above results demonstrate the synchronization stability boundary expressed by Eq.(1) can discriminate the stability of multiple swings for multiple generators in real time. More importantly, this finding suggests that the synchronous stability boundary and the multimachine multiswing stability boundary are, in fact, identical. This result helps analyze the synchronous stability of the power system in a unified way.

The numerical experimental results in Figures 1(d), (e) and (f) are time-series data independently calculated by the simulation software. The results in Figures 1(b) and (c) are in good agreement with these experimental data. The above results provide solid evidences for the correctness and validity of the boundary equation from various perspectives.

As shown in Figure 1(a), geometrically, Eq. (1) represents two surfaces in a coordinate system $u_K - u_L - \delta_{K,L}$. The left-hand side of Eq. (1) corresponds to a plane (dark green) perpendicular to the plane $u_K - u_L$, and the right-hand side corresponds to a curve surface (blue). These two surfaces are clearly fixed, i.e., they are independent of network topology and parameters. Therefore, Eq. (1) is independent of the network topology, system parameters, perturbations and number of subsystems. This finding, which contradicts previous reports[2,13,14], indicates that the stability boundary is independent of these factors. I emphasized that $\frac{|P_{\partial u}|}{|P_{\Delta u}|} = 1$, not $P_{\Delta u}$ and $P_{\partial u}$, is independent of the network topology. The impact of the network is nullified through division (refer to "Derivation of the boundary equation").

The most straightforward **method** to prove that "the boundary is independent of the network" is to test whether Eq. (1) holds true for a completely different network. Analogous results were obtained for the 3-generator test system using the same procedure (see Figure S1). Figure 1 shows the results of the simulation with the New England test system, whereas the results in Figure S1 are from the 3-generator test system. The New England test system and 3-gen are two completely different network systems. They clearly have completely different topologies and parameters, but in both cases, the same boundary equation is applied. This is because the aforementioned evidence can be reproduced in the 3-generator test system. Both Figure S1(a) and Figure 1(b) correspond to evidence 1) mentioned above. Both Figure S1(b) and Figure 1(c) correspond to evidence 2). Both Figure S1(e) and Figure 1(f) correspond to evidence 3). Consequently, a comparison of Figures 1 and S1 reveals that Eq. (1) can be used to characterize the boundary of a different network. Moreover, the failures occurring on different network nodes can lead to different network structures. That is, the results in Figure S8 can be considered as coming from different networks. These results also show that Eq. (1) is independent of the network. Eq. (1) is the analytical equation for the synchronous stability boundary. Therefore, these findings demonstrate that the synchronization stability boundary is independent of the network structure and parameters. This conclusion is at least applicable to those reconfigurable networks. Eq.(1) can be a good solution for multiple generators' synchronization stability, the stability of multiple swings for multiple generators, and partial synchronization.

More information can be obtained from the expression of Eq. (1). Specifically, the left-hand side of Eq. (1) represents the global stability domain[13] (i.e.,when $|u_L| = |u_K|$, $\forall \delta_{K,L} \geq 0, P_{\Delta u} = P_{\partial u}$).

 doi:10.20944/preprints202310.1791.v6

$|u_L| = |u_K|$ is a manifestation of the symmetry of the system. This finding shows that high symmetry can promote synchronization in complex networks. This can explain why symmetric networks have better synchronization capabilities. This has been reported in various studies[31,32].

The right-hand side of Eq. (1) has a variant that is expressed by:

$$\delta_{K,L}^{cr} = \arccos(1 - \frac{|u_K| - |u_L|}{2|u_K|}) \quad (2)$$

where $\delta_{K,L}^{cr}$ is the stability margin of the Kth and Lth meta-generator angle difference of the rotation rate. $\delta_{K,L}^{cr} \geq 0$. The difference between $|u_K|$ and $|u_L|$ can be used to measure the degree of asymmetry of the system. Clearly, when $|u_K|, |u_L|$ are sufficiently close[33], $\delta_{K,L}^{cr}$ tends to 0. As $|u_K| - |u_L|$ increases, $\delta_{K,L}^{cr}$ increases. In other words, the synchronization stability domain becomes larger as the degree of asymmetry increases. This explains the recently discovered superior synchronization stability of highly asymmetric systems[6,34]. It is very difficult to maintain a high degree of symmetry at all times after the system is perturbed. For those systems requiring stability, asymmetry may be a more economical candidate. When $\delta_{K,L}^{cr} > \frac{\pi}{3}$, the Kth and Lth meta-generators are not synchronized.

Consequently, both high symmetry and high asymmetry promote synchronization. The expression of Eq. (1) is very simple, yet it *harmonize*s these two contradictory conclusions well and requires no additional assumptions.

In summary, Eq. (1) enables a unified analysis of the synchronization stability of the grid and provides a new understanding of synchronization. To determine the stability of a power system of n generators, only n pairs of variables $u_i, \delta_i, i \in (1, 2, ..., n)$ are required. These variables are physically meaningful and can be readily obtained. This greatly simplifies the study of grid synchronization stability.

Synchronization of complex networks is one of the central concepts of complexity science. However, the expression for its stability boundary, the equation $P_{\Delta u} = P_{\partial u}$, is so simple. It may suggest that we need to further understand the concept of the "complexity".

Spontaneous Synchronization

Synchronized systems may be destabilized when they are disturbed. Therefore, it is equally important to study the the transition behavior of a disturbed system from stable to unstable states. I have observed that when the system is disturbed and on the brink of destabilization, the trajectory of the operating point becomes intriguing. A surprisingly specific structure emerges from the collective behavior of these trajectories. The operating point of the ith meta-generator is denoted by (u_i, δ_i).

(a). Spontaneous synchronization of meta-generators. The horizontal axis represents the fault clearing time. The vertical axis represents the standard deviation of δ. The yellow area means the thin layer where spontaneous synchronization occurs. Here, $\sigma(\delta_i)$ denotes the standard deviation of δ, which begins to decrease at 0.147 s (magenta dots) and increases by 1300% at 0.155 s when the system becomes unstable (cyan pentagram dots). $\sigma(\delta_i)$ can be calculated using Eq. (S6).

(b). The phenomenon of potential barrier on plane $\delta_1 - \delta_2$. Δt increased from 0.140 s to 0.154 s. The black arrow means the direction in which Δt increased. From $\Delta t = 0.147\ s$ (the magenta

 doi:10.20944/preprints202310.1791.v6

dot) onward, the distance between neighboring points decreased in the direction of the black arrow (the elliptical shaded area).

(c). Starting points of spontaneous synchronization. The horizontal axis represents the fault clearing time. The amplified points mean the starting points of spontaneous synchronization. Near the boundary, all of starting points appear at $\Delta t = 0.147\ s$. The disturbance trajectories of all of the points were almost identical. δ_i in panels (b) and (c) are calculated using Eq. (S3).

As shown in Figure 2(a), $\sigma(\delta_i)$ exhibits discontinuity at 0.154 s and 0.155 s. In agreement with the findings presented in Figure 1, the system is stable at $\Delta t = 0.154\ s$ and unstable at $\Delta t = 0.155\ s$. The decrease in $\sigma(\delta_i)$ from the highest point in the yellow region indicated that on the brink of destabilization, the velocity of the subsystem was spontaneously directed toward the mean value. This counterintuitive phenomenon is consistent with the definition of spontaneous synchronization effect[8,35]. The spontaneous synchronization effect causes $\sigma(\delta_i)$ to decrease whether the operating point crosses the potential barrier in the inward or outward direction. Therefore, within the thin layer, the results of $\sigma(\delta_i)$ in different directions are not the same. This may form a hysteresis loop of $\sigma(\delta_i)$ in these directions.

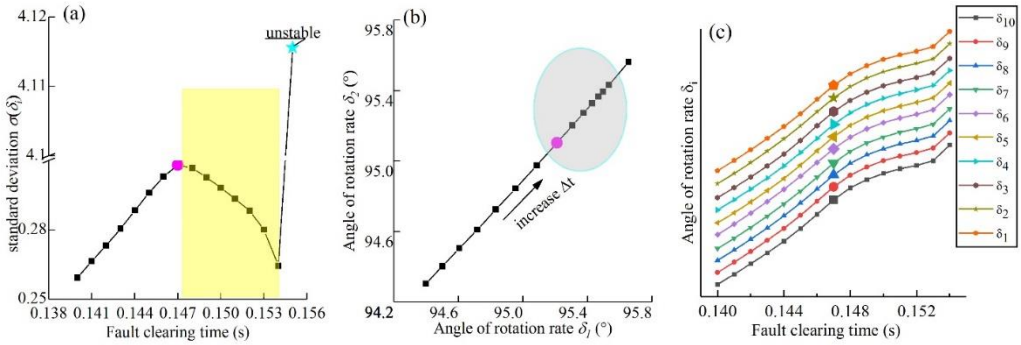

Figure 2. Spontaneous synchronization and unique structure. The fault clearing time Δt increases from 0.140 s to 0.155 s. The arrow means the direction of increase in Δt (the 18-node three-phase short circuit to the ground fault). $d(\Delta t) = 0.001\ s$.

Although spontaneous synchronization has been utilized to understand the synchronous operation of generators[23], certain studies have cast doubt on the existence of spontaneous synchronization in power systems[9]. The reason for these doubts is that current research has not uncovered direct evidence of self-organizing synchronization in the power system, nor has it shown exactly where it occurs. Self-organizing behavior emerges from the interactions of these meta-generators, and its effects are reflected in the perturbation trajectories at the operating point. As shown in Figure 2(b), for a constant step size $d(\Delta t) = 0.001\ s$, the interval between points decreases progressively within the shaded area, leading to the emergence of a unique trajectory structure. I refer to this novel structure as a "potential barrier" because the points within the shaded area exhibit "decelerating motion", as if the mass points were crossing a potential barrier. To the best of my knowledge, this structure has not been previously reported. $\sigma(\delta_i)$ reaches its maximum at $\Delta t = 0.147\ s$ and begins to decrease in Figure 2(a). The magenta dot corresponds exactly to $\Delta t = 0.147\ s$ in Figures 2(b). All of amplified points appear at the identical Δt in Figure 2(c). These amplified points are located at the transition of $\frac{d^2\delta_i}{d(\Delta t)^2}$. Prior to this, $\frac{d^2\delta_i}{d(\Delta t)^2} > 0$. After this,

 doi:10.20944/preprints202310.1791.v6

$\frac{d^2\delta_i}{d(\Delta t)^2} < 0$. Moreover, the system is unstable at $\Delta t = 0.155\ s$. These results demonstrate that $\Delta t = 0.147\ s$ is the starting point and $\Delta t = 0.154\ s$ is the end of spontaneous synchronization. This is the position of spontaneous synchronization where emergence occurs.

Currently, spontaneous synchronization is considered to be closely related to the network structure[36]. However, the results of this paper yield another conclusion. I want to emphasize that the "spontaneous synchronization" in this paper refers only to the position of spontaneous synchronization where emergence occurs. The experimental results show that the thin layer where spontaneous synchronization occurred is found only close to the synchronization stability boundary. Different failures led to different network structures. Similar to Figure 2(a), those results in Figure S5 from different network structures suggest that a decrease in $\sigma(\delta_i)$ occurs only when the system is on the brink of lose synchronization. In other words, the system suddenly self-organizes toward synchronous evolution only when it about to reach a critical synchronous stable state. Additionally, a comparison of Figures 2(a) and S2(a) indicates that the same conclusion holds true for a completely different network. These phenomenon can be interpreted as spontaneous synchronization occurring only close to the synchronous stability boundary. Eq. (1) describes the stability boundary of the power system. Consequently, for coupled network systems, the link between spontaneous synchronization and the boundary suggests that the location where spontaneous synchronization occurs is constrained by Eq. (1). As mentioned above, Eq. (1) is independent of the network. This finding suggests that spontaneous synchronization is independent of the network. This conclusion challenges the traditional perception of spontaneous synchronization in networks.

Additionally, when $P_{\Delta u} = P_{\partial u}$, collective synchronization emerges from individuals' behavior. Specifically, at $\Delta t = 0.147\ s$, $\frac{d^2\delta_i}{d(\Delta t)^2}$ of all meta-generators transforms simultaneously (refer to Figure 2(c)). Given that these meta-generators are connected to different nodes, this result suggests that they exhibit long-range correlation at the point of impending destabilization. This correlation leads to a collective movement of all individuals as a whole.

Current research on synchronization phenomena focuses on the transition from disorder to synchronization. There are few references to "the emergence of spontaneous synchronization during the evolution of a fully synchronized system to disorder". The paper shows that the system also undergoes self-organization before it loses synchronization stability. Synchronization emerges from disorder when an operating point crosses the boundary in the inward direction. In this case, spontaneous synchronization may have different initial values and conditions, and it is not clear where it is started, which is an important issue that is not discussed in this paper. Considering that u_i changes before δ_i and that $P_{\Delta u} = P_{\partial u}$ is a phase transition point, I infer that the boundary is the onset of synchronization in that case.

The behavior of the operating point near the boundary is diverse. For example, A comparison of Figures 2 and S2 reveals that spontaneous synchronization can result in at least two different results. The reasons for this difference, or rather, the specific conditions for the formation of a potential barrier, require further research. Moreover, the thin layer where spontaneous synchronization occurs has some thickness. This thickness may be related to the network topology and parameters, but its solution is not clear. These issues will be addressed in future research.

Methods

There is a consensus in the literature: Synchronization occurs when the coupling dominates the dissimilarity[2]. Currently, the coupling is typically quantified by graph theory, and the dissimilarity is quantified by the frequencies ω_i.

Preprints.org (www.preprints.org) | NOT PEER-REVIEWED | Posted: 16 January 2025 doi:10.20944/preprints202310.1791.v6

(a). The generators are kept in synchronized operation. The magenta dot indicates the ith generator $u_i\angle\delta_i$. The length of the solid cyan line represents the generator port bus voltage amplitude $|u_i|$. The angle of the solid line $\delta_i = 2\arctan(\omega_i), i = 1,2,\cdots,n$ is defined as the angle of rotation rate of the Kth meta-generator. Note that δ_i is not a phase. ω_i is the rotor speed per unit of the Kth meta-generator. Specifically, for the power system, when the generator operates synchronously, $\omega_1 = \omega_2 = \cdots = \omega_n = 1$, and $\delta_i = \frac{\pi}{2}, i = 1,2,\cdots,n$.

(b). Following a disturbance in the power system, $\omega_K \neq \omega_L$, and $\delta_{K,L} > 0$. Δu is defined as "the coupling potential difference" between the Kth and Lth meta-generators (the orange dotted line between the magenta square dots). Correspondingly, ∂u is constructed to describe "the dissimilar potential difference" between the Kth and Lth meta-generators (the solid blue line between the cyan dots).

In real operating power systems, the generator port bus voltages (per unit value) u_K and u_L are often unequal. That is, when all generators operate synchronously, the coupling strength between them is greater than 0 because of the difference between u_K and u_L (i.e., $\delta_{K,L} = 0, \Delta u = u_K - u_L > 0$)[see Figure 3(a)]. Unlike in the previous method, the coupling strength between the nodes is quantified by $P_{\Delta u}$. $P_{\Delta u}$ is the coupling power. $P_{\Delta u} > 0$.

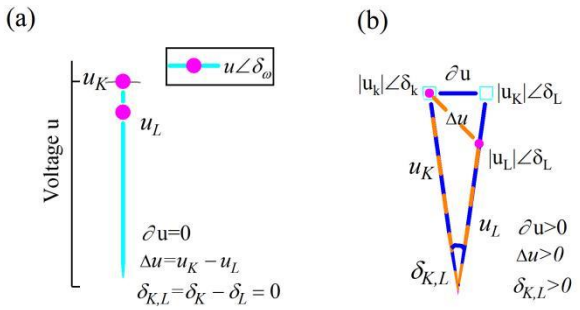

Figure 3. Schematic diagram. Figure 3 is an analogous illustration of the amplitude angle $U_i\angle\delta_i$ which is the foundation of power system analysis.

On the other hand, the dissimilarity between the nodes is quantified by $P_{\partial u}$. $P_{\partial u}$ is named the dissimilar power. $P_{\partial u} = 0$ corresponds to complete synchronization. When all the generators are completely synchronized(i.e., no dissimilarity), $P_{\partial u} = 0$ (i.e., $\delta_{K,L} = 0, \partial u = 0$). Following a disturbance in the power system, the generators' rotational speeds are dissimilar, $P_{\partial u} > 0$ (i.e., $\delta_{K,L} > 0, \Delta u > 0, \partial u > 0$) [see Figure 3(b)].

The expressions for $P_{\Delta u} = \frac{|\Delta u|^2}{|Z_{K,L}|}$ and $P_{\partial u} = \frac{|\partial u|^2}{|Z_{K,L}|}$ are analogous to those of $P_{K,L} = \frac{|\vec{U}_K - \vec{U}_L|^2}{|Z_{K,L}|}$, which can represent the interaction between the nodes in a power system. $P_{\Delta u}$

 doi:10.20944/preprints202310.1791.v6

and $P_{\partial u}$ have the same dimension and can be directly compared in size. $Z_{K,L}$ is the impedance between the Kth and Lth meta-generators.

Considering the consensus mentioned earlier, the boundary equation is expressed as $P_{\Delta u} = P_{\partial u}$ in the grid. When $|P_{\partial u}| \le |P_{\Delta u}|$, the system is synchronous and stable. Conversely, when $|P_{\partial u}| > |P_{\Delta u}|$ [to fulfill this condition, $\partial u(u_K)$ is chosen instead of $\partial u(u_L)$ in Eq. (S1)], the system is out of synchronization and unstable.

I emphasize that $\frac{|P_{\partial u}|}{|P_{\Delta u}|} = 1$, not $P_{\Delta u}$ and $P_{\partial u}$, is independent of the network topology. It is clear from the form of $P_{\Delta u}$ and $P_{\partial u}$ that they are related to the network, as information about the network is contained in $Z_{K,L}$. However, $\frac{|P_{\partial u}|}{|P_{\Delta u}|} = 1$ eliminates $Z_{K,L}$. It is observed that $\frac{|P_{\partial u}|}{|P_{\Delta u}|} = 1 \Leftrightarrow \frac{|\partial u|}{|\Delta u|} = 1$. The set of points for which $|\partial u| = |\Delta u|$ is the synchronous stability boundary.

As shown in Figure 3(b),

$$\begin{aligned} \Delta u &= \sqrt{u_K^2 + u_L^2 - 2u_K u_L \cos\delta_{K,L}}, \\ \partial u &= \sqrt{2u_K^2(1-\cos\delta_{K,L})}. \end{aligned} \tag{S1}$$

The symbols "Δ" and "∂" are for distinction only and have no mathematical significance. Thus, Eq. (1) is obtained via derivation from $u_K^2 + u_L^2 - 2u_K u_L \cos\delta_{K,L} = 2u_K^2(1-\cos\delta_{K,L})$. Clearly, the only variables in Eq. (1) are u_K, u_L and $\delta_{K,L}$.

$f\left(u_K, u_L, \delta_{K,L}\right) = \frac{|\partial u|}{|\Delta u|} = 1$ is the stability boundary equation. When $\frac{|\partial u|}{|\Delta u|} < 1$, the system is stable. When $\frac{|\partial u|}{|\Delta u|} > 1$, the system is unstable. Geometrically, $f\left(u_K, u_L, \delta_{K,L}\right) = 1$ describes exactly curved surfaces that, together with $(0, u_L, \delta_{K,L})$, $(u_K, 0, \delta_{K,L})$ and $(u_K, u_L, 0)$ encloses a stable domain.

In summary, the boundary equation $|u_K| = |u_L| \cup \frac{|u_L|}{|u_K|} = 2\cos\delta_{K,L} - 1$ can be found, where $|u_K| \ge |u_L| \ge 0, |\delta_{K,L}| \ge 0$. The coordinate system $u_K - u_L - \delta_{K,L}$ is established, and the boundary is visualized (Figure 1(a)).

Data Processing

The angle of rotation rate of the ith generator was subsequently calculated as $\delta_i'(t) = 2\arctan[\omega_i'(t)]$. The extensive interconnections between generators make stability analysis very challenging (see Figure S3). This challenge arises from the complexity of the network. To address this issue, the concept of a meta-generator is introduced here. At moment t, the instantaneous values of the n generator system $\left(u_i'(t), \delta_i'(t)\right), i = 1, 2, \cdots, n$ are arranged in descending order by δ_ω, relabeled, and then reconstituted as the n meta-generator system $\left(u_i(t), \delta_i(t)\right), i = 1, 2, \cdots, n$.

In other words, when the condition $\delta_{i+1}'(t) > \delta_i'(t)$ holds,

 doi:10.20944/preprints202310.1791.v6

$$(u_{i+1}(t),\delta_{i+1}(t))=(u_i'(t),\delta_i'(t)),$$
$$(u_i(t),\delta_i(t))=(u_{i+1}'(t),\delta_{i+1}'(t)). \tag{S2}$$

A meta-generator is created by reordering and labeling generators. This is a technical treatment only, and this transformation has been shown not to change the pattern of change in the state of the system [see Figures S4(a), S6 and S7]. In this way, I obtain the meta-generator data $(u_i(t),\delta_i(t)),i=1,2,\cdots,n$. Before and after the transformation, the number of generators and meta-generators is equal.

The operating point of the ith meta-generator is represented by (u_i,δ_i). The coupling point of the Kth and Lth meta-generators is represented by $(u_K,u_L,\delta_{K,L})$. This data can be utilized as coordinates for visualization, as shown in Figure 1. These points are calculated as follows:

The means of $(u_i(t),\delta_i(t)),i=1,2,\cdots,n$ over $[0,T]$ were

$$u_i=\frac{1}{T}\int_0^T u_i(\tau)d\tau,$$
$$\delta_i=\frac{1}{T}\int_0^T \delta_i(\tau)d\tau \tag{S3}$$

and

$$\delta_{K,L}=\frac{1}{T}\int_0^T \delta_{K,L}(\tau)d\tau=\frac{1}{T}\int_0^T \left|\delta_K'(\tau)-\delta_L'(\tau)\right|d\tau$$
$$=\frac{1}{T}\int_0^T \delta_K(\tau)-\delta_L(\tau)d\tau=\delta_K-\delta_L. \tag{S4}$$

The results here are shown in Figures 1(b), 2(b), S2(a), etc.

After disturbance, the location of the coupling point vary with time. The means of $(u_i(t),\delta_i(t)),i=1,2,\cdots,n$ over $[T,T+dT]$ were

$$u_i(dT)=\frac{1}{dT}\int_T^{T+dT} u_i(\tau)d\tau,$$
$$\delta_{K,L}(dT)=\delta_K(dT)-\delta_L(dT)=\frac{1}{dT}\int_T^{T+dT}\left[\delta_K(\tau)-\delta_L(\tau)\right]d\tau, \tag{S5}$$

where dT is the time interval. The results here are shown in Figures 1(c) and S2(b).

Near the boundary, δ_i was calculated at a relatively fine scale. The standard deviation of δ_i is calculated as follows:

$$\sigma(\delta_i)=\sqrt{\frac{\sum_{i=1}^{n}(\delta_i-E(\delta_i))^2}{n}},$$
$$E(\delta_i)=\frac{\sum_{i=1}^{n}\delta_i}{n}. \tag{S6}$$

where $E(\delta_i)$ is the expectation of δ_i. The results here are shown in Figures 2(a) and S2(a) and S5.

References

1. Koronovskii, A. A., Moskalenko, O. I. & Hramov, A. E. synchronization in complex networks. *Tech. Phys. Lett.* **38**, 924–927 (2012).

2. Dörfler, F., Chertkov, M. & Bullo, F. Synchronization in complex oscillator networks and smart grids. *Proc. Natl. Acad. Sci. U. S. A.* **110**, 2005–2010 (2013).
3. Wu, K., Hao, X., Liu, J., Liu, P. & Shen, F. Online Reconstruction of Complex Networks From Streaming Data. *IEEE Trans. Cybern.* **52**, 5136–5147 (2022).
4. Linyuan, L. L. & Zhou, T. Link prediction in complex networks: A survey. *Phys. A Stat. Mech. its Appl.* **390**, 1150–1170 (2011).
5. Xu, Y., Zhou, W. & Fang, J. Topology identification of the modified complex dynamical network with non-delayed and delayed coupling. *Nonlinear Dyn.* **68**, 195–205 (2012).
6. Molnar, F., Nishikawa, T. & Motter, A. E. Asymmetry underlies stability in power grids. *Nat. Commun.* **12**, 1–9 (2021).
7. Martínez, I., Messina, A. R. & Vittal, V. Normal form analysis of complex system models: A structure-preserving approach. *IEEE Trans. Power Syst.* **22**, 1908–1915 (2007).
8. Zhu, L. & Hill, D. J. Synchronization of Kuramoto Oscillators: A Regional Stability Framework. *IEEE Trans. Automat. Contr.* **65**, 5070–5082 (2020).
9. Casals, M. R. *et al.* Knowing power grids and understanding complexity science. *Int. J. Crit. Infrastructures* **11**, 4 (2015).
10. Gurrala, G., Dimitrovski, A., Pannala, S., Simunovic, S. & Starke, M. Parareal in Time for Fast Power System Dynamic Simulations. *IEEE Trans. Power Syst.* **31**, 1820–1830 (2016).
11. Gurrala, G. *et al.* Large Multi-Machine Power System Simulations Using Multi-Stage Adomian Decomposition. *IEEE Trans. Power Syst.* **32**, 3594–3606 (2017).
12. Wang, B., Fang, B., Wang, Y., Liu, H. & Liu, Y. Power System Transient Stability Assessment Based on Big Data and the Core Vector Machine. *IEEE Trans. Smart Grid* **7**, 2561–2570 (2016).
13. Yu, Y., Liu, Y., Qin, C. & Yang, T. Theory and Method of Power System Integrated Security Region Irrelevant to Operation States: An Introduction. *Engineering* **6**, 754–777 (2020).
14. Yang, P., Liu, F., Wei, W. & Wang, Z. Approaching the Transient Stability Boundary of a Power System: Theory and Applications. *IEEE Trans. Autom. Sci. Eng.* 1–12 (2022) doi:10.1109/TASE.2022.3213678.
15. Al-Ammar, E. A. & El-Kady, M. A. Application of operating security regions in power systems. *IEEE PES Transm. Distrib. Conf. Expo. Smart Solut. a Chang. World* (2010) doi:10.1109/TDC.2010.5484270.
16. Kundur, P. *et al.* Definition and classification of power system stability. *IEEE Trans. Power Syst.* **19**, 1387–1401 (2004).
17. Student Member, B. B. & Senior Member, G. A. On the nature of unstable equilibrium points in power systems. *IEEE Trans. Power Syst.* **8**, 738–745 (1993).
18. Chiang, H. D., Wu, F. F. & Varaiya, P. P. A BCU Method for Direct Analysis of Power System Transient Stability. *IEEE Trans. Power Syst.* **9**, 1194–1208 (1994).
19. Shubhanga, K. N. & Kulkarni, A. M. Application of Structure Preserving Energy Margin Sensitivity to Determime the Effectiveness of Shunt and Serles FACTS Devices. *IEEE Power Eng. Rev.* **22**, 57 (2002).
20. Bhui, P. & Senroy, N. Real-Time Prediction and Control of Transient Stability Using Transient Energy Function. *IEEE Trans. Power Syst.* **32**, 923–934 (2017).
21. Al Marhoon, H. H., Leevongwat, I. & Rastgoufard, P. A fast search algorithm for Critical Clearing Time for power systems transient stability analysis. *2014 Clemson Univ. Power Syst. Conf. PSC 2014* (2014) doi:10.1109/PSC.2014.6808093.
22. Rimorov, D., Wang, X., Kamwa, I. & Joos, G. An approach to constructing analytical energy function for synchronous generator models with subtransient dynamics. *IEEE Trans. Power Syst.* **33**, 5958–5967 (2018).
23. Motter, A. E., Myers, S. A., Anghel, M. & Nishikawa, T. Spontaneous synchrony in power-grid networks. *Nat. Phys.* **9**, 191–197 (2013).
24. Li, X., Wei, W. & Zheng, Z. Promoting synchrony of power grids by restructuring network topologies. *Chaos An Interdiscip. J. Nonlinear Sci.* **33**, 63149 (2023).
25. Kuramoto, Y. & Battogtokh, D. Coexistence of Coherence and Incoherence in Nonlocally Coupled Phase Oscillators. *Physics (College. Park. Md).* **4**, 380–385 (2002).
26. Martens, E. A., Thutupalli, S., Fourrière, A. & Hallatschek, O. Chimera states in mechanical oscillator networks. *Proc. Natl. Acad. Sci. U. S. A.* **110**, 10563–10567 (2013).

27. Panaggio, M. J. & Abrams, D. M. Chimera states: Coexistence of coherence and incoherence in networks of coupled oscillators. *Nonlinearity* **28**, R67–R87 (2015).
28. Ding, L., Gonzalez-Longatt, F. M., Wall, P. & Terzija, V. Two-step spectral clustering controlled islanding algorithm. *IEEE Trans. Power Syst.* **28**, 75–84 (2013).
29. Ajala, O., Dominguez-Garcia, A., Sauer, P. & Liberzon, D. A Second-Order Synchronous Machine Model for Multi-swing Stability Analysis. *51st North Am. Power Symp. NAPS 2019* (2019) doi:10.1109/NAPS46351.2019.9000368.
30. Alberto, L. F. C. & Bretas, N. G. Required damping to assure multiswing transient stability: the SMIB case. *Int. J. Electr. Power Energy Syst.* **22**, 179–185 (2000).
31. Pecora, L. M., Sorrentino, F., Hagerstrom, A. M., Murphy, T. E. & Roy, R. Cluster synchronization and isolated desynchronization in complex networks with symmetries. *Nat. Commun.* **5**, (2014).
32. Denker, M., Timme, M., Diesmann, M., Wolf, F. & Geisel, T. Breaking Synchrony by Heterogeneity in Complex Networks. *Phys. Rev. Lett.* **92**, 1–4 (2004).
33. Karatekin, C. Z. & Uçak, C. Sensitivity analysis based on transmission line susceptances for congestion management. *Electr. Power Syst. Res.* **78**, 1485–1493 (2008).
34. Nishikawa, T. & Motter, A. E. Symmetric States Requiring System Asymmetry. *Phys. Rev. Lett.* **117**, 114101 (2016).
35. Dörfler, F. & Bullo, F. Synchronization in complex networks of phase oscillators: A survey. *Automatica* **50**, 1539–1564 (2014).
36. Fan, H., Wang, Y. & Wang, X. Eigenvector-based analysis of cluster synchronization in general complex networks of coupled chaotic oscillators. *Front. Phys.* **18**, (2023).
37. Anderson, P. M. & Fouad, A. A. *Power System Control and Stability*. (John Wiley & Sons, 2008).
38. Pai, A. *Energy Function Analysis for Power System Stability*. (Springer Science & Business Media, 1989).
39. NIU, M., WAN, C. & XU, Z. A review on applications of heuristic optimization algorithms for optimal power flow in modern power systems. *J. Mod. Power Syst. Clean Energy* **2**, 289–297 (2014).